

Two-Photon Absorption in Silicon Using Real Density Matrix Approach

David Ziemkiewicz,¹ David Knez,² Evan P. Garcia,² Sylwia Zielińska-Raczyńska,¹ Gerard Czajkowski,¹ Alessandro Salandrino,³ Sergey S. Kharintsev, Aleksei I. Noskov,⁴ Eric O. Potma,² and Dmitry A. Fishman^{2,*}

¹*Institute of Mathematics and Physics, Technical University of Bydgoszcz,
Al. Prof. S. Kaliskiego 7, 85-789 Bydgoszcz, Poland*

²*Department of Chemistry, University of California, Irvine, Irvine, California, 92697, USA*

³*Department of Electrical Engineering, University of Kansas, Lawrence, Kansas, 66045*

⁴*Institute of Physics, Kazan Federal University, Kazan 420008, Russia*

(Dated: March 5, 2024)

Two-photon absorption in indirect gap semiconductors is an frequently encountered, but not well-understood phenomenon. To address this, the Real Density Matrix Approach is applied to describe two-photon absorption in silicon through the excitonic response to the interacting fields. This approach produces an analytical expression for the dispersion of the two-photon absorption coefficient for indirect-gap materials, and can be used to explain trends in reported experimental data for bulk silicon both old and new with minimal fitting.

I. INTRODUCTION

Two-photon absorption (2PA) is a nonlinear optical phenomenon in which the combined energy carried by two incident photons is near-instantaneously absorbed by a material. Because of its nonlinear intensity dependence, the 2PA process is spatially confined when focused light is used, thus making it possible to use the effect as a local probe in the material for imaging [1], micro-fabrication [2, 3] or three-dimensional data storage [4]. In semiconducting materials, the 2PA phenomenon produces charge carriers than can be read out electronically, a mechanism that has been used extensively for measuring the envelopes of ultrashort optical pulses. [5, 6] The use of semiconductors as 2PA detectors is particularly attractive in the case of non-degenerate two-photon absorption (NTA), in which case the energies of $\hbar\omega_a$ and $\hbar\omega_b$ of the two photons in the interaction can be vastly different, enabling the registration of individual photon energies that are well below the bandgap energy of the semiconducting material. For instance, the NTA process has made it possible to detect mid-infrared (MIR) photons with wide-bandgap semiconductors such as GaAs [7] and Si [8], thereby circumventing thermal noise issues that have plagued traditional MIR photodetectors based on low-energy bandgap materials. Moreover, the NTA principle has also been shown to enable rapid MIR imaging with high-definition visible/near-IR cameras [9–11], thereby overcoming several persistent limitations of conventional MIR cameras.

The recent developments in NTA-based imaging underline the potential of this nascent detection technology, particularly as it concerns the use of Si-based cameras for versatile imaging in the MIR range. [9, 11] From a commercial point of view, silicon is an attractive material because of its ubiquity as a feedstock and the mature technology for Si-device fabrication. On the other hand,

silicon is an indirect semiconductor that has a much lower 2PA absorption coefficient compared to direct semiconductor in the same spectral range. The main reason for silicon's lower performance as a 2PA material is the additional involvement of lattice phonons for providing the momentum needed in the indirect transition, which lowers the transition probability.

Improving the 2PA response of Si-based photodetectors requires a better understanding of the indirect two-photon transition in silicon. Reasonable progress has been made in describing degenerate and non-degenerate two-photon absorption in *direct* bandgap semiconductors. Current models compute the 2PA transition rate in such materials through a second-order perturbation of stationary material states [12–14], or via evolving Volkov-type wavefunctions in the context of first-order perturbation theory. [15] These approaches have successfully produced expressions that generally predict the energy scaling of the two-photon absorption coefficient in direct bandgap materials, including the expected enhancement of the 2PA effect in the case of extremely non-degenerate photon energies. [7] Existing models are flexible with respect to the input band structure, but do not incorporate dephasing mechanisms explicitly, and extra care must be taken to account for material anisotropy. [16] Alternative formulations include the use of semiconductor Bloch equations, which have been evaluated in the framework of the density operator that is better equipped to account for relaxation and dephasing mechanisms. [17–19]

The description of 2PA in indirect semiconductors such as silicon has so far relied heavily on the theoretical models developed for direct bandgap materials. For instance, to account for the interaction vertex with lattice phonons, higher order perturbative expansions of stationary [20, 21] or dressed states [22] have been developed to derive expressions for the nonlinear absorption coefficient. Although such models reproduce the general behaviour of measured two-photon absorption coefficients, quantitative matching between experiment and theory has proven more challenging. Recently,

* dmitryf@uci.edu

Faryadraz et al. obtained a semi-empirical scaling law for NTA coefficients, which was compared with experimental data. [23]. While semi-empirical models can be useful for gaining mechanistic insights, a more complete theory of two-photon absorption in indirect bandgap materials is needed to quantitatively predict the scaling of 2PA coefficients over a wide range of the energy ratio $\hbar\omega_b/\hbar\omega_a$.

In this work, we advance the theoretical description of the two-photon absorption process in silicon through the application of the real density matrix approach (RDMA). This approach has been successful in describing linear and nonlinear optical properties of semiconductors in terms of Rydberg excitons for the case of one-photon excitation [24, 25]. The RDMA method allows the use of a small number of well-known parameters (e.g., effective masses, gap energy, dielectric constant) to derive expressions for the optical response of the material. Here, we adapt the RDMA for the case of two-photon excitation in semiconductors, extending it for the case of silicon to include both excitonic and continuum states, as well as lattice phonons for momentum matching. Using this approach, we derive analytical expressions for the two-photon coefficient while including dephasing times and anisotropy of the material under study. We compare the energy scaling of the predicted NTA coefficient with published experimental data, supplemented with new experimental data, and demonstrate excellent quantitative agreement over a broad range of $\hbar\omega_b/\hbar\omega_a$ dispersion values.

II. THEORY

A. Real density matrix approach

In the RDMA approach the nonlinear response is described by a set of coupled equations for the exciton density represented by the coherent amplitude $Y(\mathbf{r}_1, \mathbf{r}_2)$, the density matrix for the conduction electrons $C(\mathbf{r}_1, \mathbf{r}_2)$, and the density matrix $D(\mathbf{r}_1, \mathbf{r}_2)$ for the holes in the valence band. [24]. These matrices are sub-matrices of the following density matrix

$$\hat{\underline{\rho}} = \begin{pmatrix} C & Y^* \\ Y & 1 - D \end{pmatrix}. \quad (1)$$

The evolution of the system is described by Heisenberg equation for the density matrix $\frac{\delta \hat{\underline{\rho}}}{\delta t} = [\hat{\underline{\rho}}, \hat{H}]$, supplemented by relaxation terms. We also define the excitonic center-of-mass coordinate

$$\mathbf{R} = \mathbf{R}_{12} = \frac{m_h \mathbf{r}_1 + m_e \mathbf{r}_2}{m_h + m_e}, \quad (2)$$

and $\mathbf{r} = \mathbf{r}_1 - \mathbf{r}_2$ is the electron-hole relative coordinate.

The Hamiltonian consists of two parts

$$\hat{H} = H_{eh} + H', \quad (3)$$

where H_{eh} is the electron-hole Hamiltonian [24], and H' describes the exciton-phonon interaction

$$H' = a(\mathbf{q}) e^{-i\omega_{ph}t} V_p(\mathbf{q}, \mathbf{r}) + \text{c.c.}, \quad (4)$$

where

$$V_p(\mathbf{q}, \mathbf{r}) = \left(\frac{\hbar}{2M\omega_{ph}} \right)^{1/2} \times \sum_{\mathbf{R}_a} e^{i\mathbf{q}\mathbf{R}_a} \mathbf{e}_0 \cdot \nabla_r V(\mathbf{r} - \mathbf{R}_a). \quad (5)$$

The $a(\mathbf{q})$ is the phonon annihilation operator, $V(\mathbf{r} - \mathbf{R}_a)$ is the potential at the point \mathbf{R}_a , \mathbf{e}_0 is the phonon polarization, ω_{ph} is the phonon frequency and \mathbf{q} is its wave vector.

The constitutive equations for the Y , C and D matrices have the following form

$$i\hbar\partial_t Y - H Y = -\mathbf{M}\mathbf{E} + \mathbf{E}\mathbf{M}_0 C + \mathbf{E}\mathbf{M}_0 D + i\hbar \left(\frac{\partial Y}{\partial t} \right)_{\text{irrev}}, \quad (6)$$

$$i\hbar\partial_t C + H_{ee} C = \mathbf{M}_0 \mathbf{E} (Y - Y^*) + i\hbar \left(\frac{\partial C}{\partial t} \right)_{\text{irrev}}, \quad (7)$$

$$i\hbar\partial_t D - H_{hh} D = \mathbf{M}_0 \mathbf{E} (Y - Y^*) + i\hbar \left(\frac{\partial D}{\partial t} \right)_{\text{irrev}}, \quad (8)$$

where the smeared-out transition dipole density $\mathbf{M}(\mathbf{r})$ and its integrated strength \mathbf{M}_0 are related to the bilocality of the amplitude Y and describe the quantum coherence between the macroscopic electromagnetic field and the inter-band transitions. The electron-electron and hole-hole interaction Hamiltonians H_{ee} and H_{hh} were defined in reference [24]. In expressions (6)-(8), the electromagnetic field \mathbf{E} includes two frequencies ω_a and ω_b , and is written as

$$\mathbf{E} = \mathbf{E}_{0a} \exp(i\mathbf{k}_a \mathbf{R} - i\omega_a t) + \mathbf{E}_{0b} \exp(i\mathbf{k}_b \mathbf{R} - i\omega_b t) + \text{c.c.} \quad (9)$$

The terms $(\frac{\partial \dots}{\partial t})_{\text{irrev}}$ describe the dissipation and relaxation processes, and satisfy

$$\left. \frac{\partial \hat{\underline{\rho}}}{\partial t} \right|_{\text{irrev}} = = - \left(\frac{1}{T_1} [C(t) - C^{(0)}] \frac{1}{T_2} [Y^*(t) - Y^{*(0)}] \right) \left(\frac{1}{T_1} [Y(t) - Y^{(0)}] \frac{1}{T_2} [D(t) - D^{(0)}] \right). \quad (10)$$

where the states with superscript (0) represent the steady state solutions. The times T_1, T_2 describe the characteristic duration of all dephasing processes: electron-electron, electron-phonon, and electron-photon interactions. Here, T_1, T_2 are taken as phenomenological constants.

The excitonic part of the medium's polarization is obtained from

$$\begin{aligned} \mathbf{P}(\mathbf{R}, t) &= 2 \int d^3 r \mathbf{M}^*(\mathbf{r}) \text{Re } Y(\mathbf{R}, \mathbf{r}, t) \\ &= \int d^3 r \mathbf{M}^*(\mathbf{r}) [Y(\mathbf{R}, \mathbf{r}, t) + \text{c.c.}] \end{aligned} \quad (11)$$

The linear optical properties are calculated by solving the interband equation (6), supplemented by the corresponding Maxwell equation, where the polarization (11) acts as a source. For computing the nonlinear optical properties we use the entire set of constitutive equations (6)-(8). Although finding a general solution of the equations is challenging, in special situations a solution can be found. For example, if one assumes that the matrices Y, C and D can be expanded in powers of the electric field \mathbf{E} , an iterative procedure can be used.

In general, solving for Y, C and D in the context of two-photon absorption depends on the relation between the incoming frequencies ω_a, ω_b (and thus energies $\hbar\omega_a, \hbar\omega_b$) and the fundamental gap energy E_g , which enters as a parameter in the electron-hole Hamiltonian. We consider two relevant cases, to be discussed separately

1. When $\hbar\omega_a + \hbar\omega_b < 2E_g$, the excitation of discrete excitonic states is possible. Therefore we seek solutions in terms of eigenfunctions and eigenvalues of the electron-hole Hamiltonian, taking also into account the phonons.
2. In the energy range $\hbar\omega_a + \hbar\omega_b > 2E_g$, we solve the equations (14), (35) and following equations for the matrices C, D assuming $V_{eh} = 0$ [24], thus entering the energy range represented by continuum states. The solution is obtained in terms of an appropriate Green function.

B. Discrete states

Our goal is to derive expressions for the NTA absorption coefficients. These can be obtained from the third-order nonlinear susceptibility, which, in turn, can be determined via an iterative procedure within the context of the RDMA. The first step in the iteration consists of solving the equation (6), which at this stage takes on the form

$$i\hbar\partial_t Y^{(1)} - H_{eh}Y^{(1)} = -\mathbf{M}\mathbf{E} + i\hbar\left(\frac{\partial Y^{(1)}}{\partial t}\right)_{\text{irrev}}. \quad (12)$$

For the irreversible part we assume the simple form

$$\left(\frac{\partial Y^{(1)}}{\partial t}\right)_{\text{irrev}} = -\frac{1}{T_2}Y. \quad (13)$$

In the discussion of nonlinear effects we also take into account the non-resonant parts of the amplitude Y . The excitonic density Y will consist of two parts, Y_a, Y_b . Therefore, Eq.(12) generates four equations: a pair for an amplitude Y_a : one for $Y_{a-}^{(1)} \propto \exp(-i\omega_a t)$, and the second for $Y_{a+}^{(1)} \propto \exp(i\omega_a t)$

$$i\hbar\left(i\omega_a + \frac{1}{T_2}\right)Y_{a+}^{(1)} - H_{eh}Y_{a+}^{(1)} = -\mathbf{M}\mathbf{E}_a^*(\mathbf{R}, t), \quad (14)$$

$$i\hbar\left(-i\omega_a + \frac{1}{T_2}\right)Y_{a-}^{(1)} - H_{eh}Y_{a-}^{(1)} = -\mathbf{M}\mathbf{E}_a(\mathbf{R}, t),$$

and similar equations for $Y_{b\pm}^{(1)}$. In the following, we consider only one component of the vectors \mathbf{E}, \mathbf{P} and \mathbf{M} .

For the case of discrete exciton states, the exciton density in the first step is found as

$$Y_{da-}^{(1)} = E_a(\mathbf{R}, t) \sum_n \frac{c_n \varphi_n(\mathbf{r})}{\hbar(\Omega_n - \omega_a - i/T_{2n})},$$

$$Y_{da+}^{(1)} = E_a^*(\mathbf{R}, t) \sum_n \frac{c_n \varphi_n(\mathbf{r})}{\hbar(\Omega_n + \omega_a - i/T_{2n})}, \quad (15)$$

and similar expressions for $Y_{db\pm}^{(1)}$. The subscript ‘‘d’’ indicates the case of discrete excitonic states. In equations (15), we define

$$c_{n00} \equiv c_n = \int d^3r M(\mathbf{r}) \varphi_{n00}(\mathbf{r}),$$

$$\hbar\Omega_{n00} = \hbar\Omega_n = E_g + E_n(\gamma_a), \quad (16)$$

$$\varphi_{n\ell m} = R_{n\ell}(r)Y_{\ell m}(\theta, \phi),$$

where $R_{n\ell}$ are the hydrogen radial functions of an anisotropic Schrödinger equation, $Y_{\ell m}(\theta, \phi)$ are spherical harmonics, $E_{n\ell m}$ the corresponding eigenvalues

$$E_{n\ell m} = -\frac{\eta_{\ell m}^2(\gamma_a)R^*}{n^2}, \quad n = 1, 2, \dots,$$

$$\ell = 0, 1, 2, \dots, n-1, \quad m = 0, \pm 1, \pm 2, \dots, \pm \ell, \quad (17)$$

R^* is the effective excitonic Rydberg energy

$$R^* = \frac{\mu_{\parallel} e^4}{2(4\pi\epsilon_0\sqrt{\epsilon_{\parallel}\epsilon_z})^2\hbar^2}, \quad (18)$$

the anisotropy parameter γ_a is defined as

$$\gamma_a = \frac{\mu_{\parallel}\epsilon_{\parallel}}{\mu_z\epsilon_z},$$

and $\eta_{\ell m}(\gamma_a)$ is given by the following expression

$$\eta_{\ell m}(\gamma_a) = \int_0^{2\pi} d\phi \int_0^{\pi} \frac{|Y_{\ell m}|^2 \sin\theta d\theta}{\sqrt{\sin^2\theta + \gamma_a \cos^2\theta}}.$$

At room temperature, given the relatively low binding energy of excitons in Si (15 meV [26]), only the lowest excitonic state is relevant. Thus, one may assume $n = 1, \ell = m = 0$ and a single lifetime $T_{2n, n=1} = T_2$.

The solutions for $Y_{da, b\pm}^{(1)}$ determined above allow the calculation of the linear polarization

$$P^{(1)}(\omega) = \int d^3r \left[Y_{da-}^{(1)} + Y_{da+}^{(1)*} \right] M^*(\mathbf{r})$$

$$+ \int d^3r \left[Y_{db-}^{(1)} + Y_{db+}^{(1)*} \right] M^*(\mathbf{r})$$

$$= \frac{E_{0a}}{\hbar} \frac{2|c_1|^2\Omega_1}{\Omega_1^2 - (\omega_a + i/T_2)^2}$$

$$+ \frac{E_{0b}}{\hbar} \frac{2|c_1|^2\Omega_1}{\Omega_1^2 - (\omega_b + i/T_2)^2}$$

$$= \epsilon_0\chi_d^{(1)}(\omega_a)E_{0a} + \epsilon_0\chi_d^{(1)}(\omega_b)E_{0b}. \quad (19)$$

The susceptibilities defined in equation (19) can be expressed in terms of the band parameters and, for energies below the gap, when spatial dispersion is neglected, we obtain

$$\chi_d^{(1)}(\omega_j) = \epsilon_b \frac{f_1 \Delta_{LT}/R^*}{(E_{T1} - \hbar\omega_j - i\Gamma_1)/R^*}, \quad (20)$$

where $\Gamma_1 = \hbar/T_2$, and E_T is the energy of the first exciton resonance. The anisotropy-dependent oscillator strength f_1 has the form

$$f_1 = \frac{\eta_{00}^3(1 - \eta_0 r_0/a^*)}{(1 + \eta_{00} r_0/a^*)^4}. \quad (21)$$

The above formula is obtained when the dipole density $M(\mathbf{r})$ is assumed in the form

$$M(\mathbf{r}) = M_0 \frac{1}{\sqrt{4\pi}} \frac{1}{r r_0^2 \gamma_a^{1/2}} e^{-r/r_0} Y_{00}(\theta, \phi), \quad (22)$$

where $r_0 = (2\mu E_g/\hbar^2)^{-1/2}$ is the so-called coherence radius. The longitudinal transverse splitting of the ground state is

$$\frac{\Delta_{LT}}{R^*} = 2 \frac{2\mu_{\parallel}}{\epsilon_0 \epsilon_b \pi a^* \hbar^2} M_0^2, \quad (23)$$

and is $f_n \Delta_{LT}$ for the excited states. Treating Δ_{LT} as a known quantity, the above relation determines the dipole matrix element M_0 .

To obtain the nonlinear response, the solutions for $Y_{da,b\pm}^{(1)}$ are inserted as a source term in the conduction band equation (7) and the valence band equation (8). Note that each of these equations depend on the electromagnetic field. If the irreversible terms are well defined, the equations (7,8) can be solved, and this second step of the iteration yields expressions for the density matrices C and D . These density matrices can then, in turn, be used as a source term for equation (6), which can be solved to obtain expressions for $Y_{da,b\pm}^{(3)}$ in the final step of the iteration.

Account for the presence of phonons, we obtain the nonlinear polarization for the region of discrete states. We separate the polarization related to the emission of a phonon (subscript “em”), and to the absorption of a phonon (subscript “abs”). The emission contribution has the form

$$P_{d,em}^{(3)}(\omega_a, \omega_b) = P_{da,em}^{(3)} e^{-i\omega_a t} + P_{db,em}^{(3)} e^{-i\omega_b t}, \quad (24)$$

where the polarization amplitudes are defined by

$$\begin{aligned} P_{da,em}^{(3)} &= \epsilon_0 \chi_{d,self,em}^{(3)}(\omega_a, \omega_a) |E(\omega_a)|^2 E(\omega_a) \\ &+ \epsilon_0 \chi_{d,cross,em}^{(3)}(\omega_a, \omega_b) |E(\omega_b)|^2 E(\omega_a), \\ P_{db,em}^{(3)} &= \epsilon_0 \chi_{d,self,em}^{(3)}(\omega_b, \omega_b) |E(\omega_b)|^2 E(\omega_b) \\ &+ \epsilon_0 \chi_{d,cross,em}^{(3)}(\omega_b, \omega_a) |E(\omega_a)|^2 E(\omega_b), \end{aligned}$$

The nonlinear susceptibilities have the form

$$\begin{aligned} \chi_{d,self,em}^{(3)}(\omega_j, \omega_j) &= -(n_{ph} + 1) \frac{2M_0^2}{\epsilon_0} \frac{1}{T_2} \left(T_1 + \frac{i\hbar\delta(\omega - 2\omega_j)}{\hbar\omega + i\hbar/T_1} \right) \\ &\times \sum_{\ell} \frac{c_{\ell}(A_{\ell} + B_{\ell})\hbar\Omega_{\ell,em}}{(\hbar\Omega_{\ell,em})^2 - (\hbar\omega_j + i\hbar T_2^{-1})^2} \\ &\times \sum_n \frac{c_n \varphi_n(0)}{(\hbar\Omega_{n,em} - \hbar\omega_j)^2 + (\hbar/T_2)^2}, \end{aligned} \quad (25)$$

$$\begin{aligned} \chi_{d,cross,em}^{(3)}(\omega_a, \omega_b) &= -(n_{ph} + 1) \frac{2M_0^2}{\epsilon_0} \left(\frac{T_1}{T_2} \right) \\ &\times \sum_{\ell} \frac{c_{\ell}(A_{\ell} + B_{\ell})\hbar\Omega_{\ell,em}}{(\hbar\Omega_{\ell,em})^2 - (\hbar\omega_a + i\hbar T_2^{-1})^2} \\ &\times \sum_n \frac{c_n \varphi_n(0)}{(\hbar\Omega_{n,em} - \hbar\omega_b)^2 + (\hbar/T_2)^2}, \end{aligned} \quad (26)$$

and the additional cross term $\chi_{d,cross,em}^{(3)}(\omega_b, \omega_a)$ is obtained by permuting the frequencies ω_a and ω_b in equation (26). The number of available phonons n_{ph} is estimated by the formula

$$n_{ph} = \frac{1}{|\exp \frac{\hbar\omega_{ph}}{k_B \mathcal{T}} - 1|}, \quad (27)$$

with k_B is the Boltzmann constant, and \mathcal{T} the temperature. $\hbar\Omega_{n,em,abs}$ are the exciton resonance energies that include the phonon energies $\hbar\omega_{ph}$,

$$\hbar\Omega_{n,em,abs} = E_g + E_n \pm \hbar\omega_{ph}, \quad (28)$$

where “+” stands for phonon emission and “-” for phonon absorption. As discussed in [27, 28], the phonon density of states contains two local maxima at 20 meV and 60 meV, respectively, with a weighted average of approximately 40 meV. This simplified approach of taking an estimate of the average phonon energy has been used in previous calculations, providing proper fits to experimental data.

The coefficients A_{ℓ}, B_{ℓ} in equations (25,26) are related to the irreversible terms in the equations (7,8), and have the form

$$\begin{aligned} A_{\ell} &= \int d^3r \varphi_{\ell}(\mathbf{r}) e^{-r^2/2\lambda_{th,e}^2}, \quad \ell = 1, 2, \dots, \\ B_{\ell} &= \int d^3r \varphi_{\ell}(\mathbf{r}) e^{-r^2/2\lambda_{th,h}^2}, \end{aligned} \quad (29)$$

where $\lambda_{th,e}, \lambda_{th,h}$ are the so-called thermal lengths for electrons and holes, respectively,

$$\lambda_{th,e} = \left(\frac{\hbar^2}{m_e k_B \mathcal{T}} \right)^{1/2}, \quad \lambda_{th,h} = \left(\frac{\hbar^2}{m_h k_B \mathcal{T}} \right)^{1/2}.$$

The above expressions are valid when

$$\hbar\omega < E_g + \hbar\omega_{ph}.$$

For $\hbar\omega > E_g + \hbar\omega_{ph}$ one should replace $n_{ph} + 1$ by

$$\mathcal{C}(\hbar\omega - E_g - \hbar\omega_{ph})^2(n_{ph} + 1). \quad (30)$$

where \mathcal{C} is a constant. [29]

Analogous expressions can be obtained for the susceptibilities related to the phonon absorption

$$\begin{aligned} \chi_{d, \text{self,abs}}^{(3)}(\omega_j, \omega_j) &= -n_{ph} \frac{2M_0^2}{\epsilon_0} \frac{1}{T_2} \left(T_1 + \frac{i\hbar\delta(\omega - 2\omega_j)}{\hbar\omega + i\hbar/T_1} \right) \\ &\times \sum_{\ell} \frac{c_{\ell}(A_{\ell} + B_{\ell})\hbar\Omega_{\ell,abs}}{(\hbar\Omega_{\ell,abs})^2 - (\hbar\omega_j + i\hbar T_2^{-1})^2} \\ &\times \sum_n \frac{c_n \varphi_n(0)}{(\hbar\Omega_{n,abs} - \hbar\omega_j)^2 + (\hbar/T_2)^2}, \end{aligned} \quad (31)$$

$$\begin{aligned} \chi_{d, \text{cross,abs}}^{(3)}(\omega_a, \omega_b) &= -n_{ph} \frac{2M_0^2}{\epsilon_0} \left(\frac{T_1}{T_2} \right) \\ &\times \sum_{\ell} \frac{c_{\ell}(A_{\ell} + B_{\ell})\hbar\Omega_{\ell,abs}}{(\hbar\Omega_{\ell,abs})^2 - (\hbar\omega_a + i\hbar T_2^{-1})^2} \\ &\times \sum_n \frac{c_n \varphi_n(0)}{(\hbar\Omega_{n,abs} - \hbar\omega_b)^2 + (\hbar/T_2)^2}, \end{aligned} \quad (32)$$

plus the additional cross term $\chi_{d, \text{cross,abs}}^{(3)}(\omega_b, \omega_a)$ obtained by permuting the input frequencies in (32). The above expressions are valid when

$$\hbar\omega < E_g - \hbar\omega_{ph}.$$

Otherwise, n_{ph} should be replaced by

$$\mathcal{C}(\hbar\omega - E_g + \hbar\omega_{ph})^2 n_{ph}. \quad (33)$$

In section IID, we use the expressions for the nonlinear susceptibility above to determine the nonlinear absorption coefficients in silicon.

C. Continuum states

If $(\hbar\omega - \hbar\omega_{ph}) > E_g$ for the case of phonon emission, or $(\hbar\omega + \hbar\omega_{ph}) > E_g$ for the case of phonon absorption, then there is no generation of bound exciton states, and continuum states constitute the final states instead. In this case, $Y^{(1)}$ is calculated in the first iteration step by setting $V_{eh} = 0$ in the electron-hole Hamiltonian [24], giving rise to equations of the form

$$\left(E_g \pm \hbar\omega \pm \hbar\omega_{ph} - i\Gamma - \frac{\hbar^2}{2\mu} \nabla^2 \right) Y_{\pm} = \mathbf{M}(\mathbf{r}) \mathbf{E} \quad (34)$$

Equation (34) can be solved by means of the appropriate Green function

$$Y_{\pm}^{(1)} = \int d^3 r' g_{\pm}(r, r') \mathbf{M}(r', \theta, \phi) \mathbf{E}, \quad (35)$$

where

$$g_{\pm}(r, r') = \frac{2\mu}{\hbar^2} \frac{\sinh \kappa_{\pm} r^{<}}{4\pi \kappa_{\pm} r^{<} r^{>}} e^{-\kappa_{\pm} r^{>}}, \quad (36)$$

$r^{<} = \min(r, r')$ and $r^{>} = \max(r, r')$, and

$$\kappa_{\pm}^2 = \frac{2\mu}{\hbar^2} (E_g \pm \hbar\omega \pm \hbar\omega_{ph} - i\Gamma). \quad (37)$$

Assuming a linear polarization and the wave vector \mathbf{E} having a component E_0 in a direction α , simultaneously with the dipole density \mathbf{M} having a component M_0 in the same direction and, for simplicity, using the dipole density of the form

$$M(\mathbf{r}) = \frac{M_0 \delta(r - r_0)}{4\pi r_0^2} e^{-r/r_0}$$

we obtain

$$Y_{\pm}^{(1)} = M_0 E_0 g_{\pm}(r, r_0). \quad (38)$$

We may again define amplitudes of the form $Y_{ca\pm}^{(1)}, Y_{cb\pm}^{(1)}$, where the subscript ‘‘c’’ now indicates the involvement of continuum states. If, in the case of phonon emission, we encounter $\kappa^2 < 0$, we introduce

$$\kappa = -i\tilde{\kappa}, \quad (39)$$

where

$$\tilde{\kappa}_-^2 = \hbar\omega - \hbar\omega_{ph} - E_g + i\Gamma,$$

and, in this case, the Green function takes on the form

$$g_-(r, r') = \frac{2\mu}{\hbar^2} \frac{\sin \tilde{\kappa}_{\pm} r^{<}}{4\pi \tilde{\kappa}_{\pm} r^{<} r^{>}} e^{i\tilde{\kappa}_{\pm} r^{>}}. \quad (40)$$

The linear terms for the case of phonon emission and absorption and input frequency ω_a are found as

$$\begin{aligned} Y_{ca-,em}^{(1)}(r) &= M_0 E_0 a g_{a-,em}(r, r_0), \\ Y_{ca-,abs}^{(1)}(r) &= M_0 E_0 a g_{a-,abs}(r, r_0), \end{aligned} \quad (41)$$

with

$$\begin{aligned} g_{a-,em}(r, r_0) &= \frac{2\mu_{\parallel H}}{\hbar^2} \frac{\sin(\tilde{\kappa}_{a-,em} r^{<})}{4\pi \tilde{\kappa}_{a-,em} r r_0} e^{i\tilde{\kappa}_{a-,em} r^{>}}, \\ \tilde{\kappa}_{a-,em}^2 &= \frac{2\mu_{\parallel H}}{\hbar^2} [\hbar\omega_a - (E_g + \hbar\omega_{ph})] + i \frac{2\mu_{\parallel H}}{\hbar^2} \frac{\hbar}{T_2}. \end{aligned}$$

Similar expressions can be obtained for the amplitudes at input frequencies ω_b . The linear amplitudes thus obtained form the source for calculating the C and D matrices, followed by third step to determine $Y_{ca,b\pm}^{(3)}$, similar to the procedure described in section IIB. Once the $Y_{ca,b\pm}^{(3)}$ amplitudes are found, for both the phonon emission and absorption process, we may write the nonlinear cross susceptibility for the continuum states can as

$$\chi_{c,cross}^{(3)} = \chi_{c,cross,em}^{(3)}(\omega_a, \omega_b) + \chi_{c,cross,abs}^{(3)}(\omega_a, \omega_b), \quad (42)$$

with

$$\begin{aligned} \chi_{c,\text{cross,em}}^{(3)}(\omega_a, \omega_b) &= \\ &= -(n_{ph} + 1) \frac{2}{\epsilon_0} 2 \frac{T_1}{\hbar} M_0^4 \left(\frac{2\mu_{\parallel H}}{\hbar^2} \right)^2 \\ &\times \frac{1}{4\pi r_0} \left(\frac{\sin(\tilde{\kappa}_{a-,em} r_0)}{\tilde{\kappa}_{a-,em} r_0} \right)^2 \\ &\times [\tilde{\kappa}_{b-,em} r_0 + \tilde{\kappa}_{b-,abs} r_0] (A_e + A_h), \end{aligned} \quad (43)$$

$$\begin{aligned} \chi_{c,\text{cross,abs}}^{(3)}(\omega_a, \omega_b) &= \\ &= -n_{ph} \frac{2}{\epsilon_0} 2 \frac{T_1}{\hbar} M_0^4 \left(\frac{2\mu_{\parallel H}}{\hbar^2} \right)^2 \\ &\times \frac{1}{4\pi r_0} \left(\frac{\sin(\tilde{\kappa}_{a-,abs} r_0)}{\tilde{\kappa}_{a-,abs} r_0} \right)^2 \\ &\times [\tilde{\kappa}_{b-,em} r_0 + \tilde{\kappa}_{b-,abs} r_0] (A_e + A_h), \end{aligned} \quad (44)$$

where

$$\begin{aligned} \tilde{\kappa}_{j-,em} r_0 &= \left(x_j - \frac{E_g + \hbar\omega_{ph}}{E_g} \right)^{1/2}, \\ \tilde{\kappa}_{j-,abs} r_0 &= \left(x_j - \frac{E_g - \hbar\omega_{ph}}{E_g} \right)^{1/2}, \end{aligned}$$

Here A_e, A_h correspond to the expressions (29), related to the irreversible processes

$$\begin{aligned} A_e &= A'_e + iA''_e = \int d^3r' g_{a-}(r_0, r') f_{0e}(r') \\ &= 4\pi \frac{2\mu_{\parallel}}{\hbar^2} \frac{\sin(\kappa_a r_0)}{\kappa_a r_0} \int_{r_0}^{\infty} r dr e^{i\kappa_a r} e^{-r^2/\lambda_{th,e}^2} \end{aligned}$$

with an analogous expression for A_h .

D. Nonlinear absorption coefficients

The propagation of the field components E_{0a} and E_{0b} in the semiconductor follow from the wave equation with $P^{(3)}$ as a source term, which, after making the well-known slowly varying amplitude approximation, yield the following coupled equations for the field amplitudes

$$\begin{aligned} \frac{\partial E_{0a}}{\partial z} &= i \frac{\omega_a}{n_a c} \chi_{\text{self}}^{(3)}(\omega_a, \omega_a) |E_{0a}|^2 E_{0a} \\ &+ i \frac{\omega_a}{n_a c} \chi_{\text{cross}}^{(3)}(\omega_a, \omega_b) |E_{0b}|^2 E_{0a}, \end{aligned} \quad (45)$$

$$\begin{aligned} \frac{\partial E_{0b}}{\partial z} &= i \frac{\omega_b}{n_b c} \chi_{\text{self}}^{(3)}(\omega_b, \omega_b) |E_{0b}|^2 E_{0b} \\ &+ i \frac{\omega_b}{n_b c} \chi_{\text{cross}}^{(3)}(\omega_b, \omega_a) |E_{0a}|^2 E_{0b}. \end{aligned} \quad (46)$$

From the equation above, the intensities of the input beams can be found as

$$\begin{aligned} I_a &= 2\epsilon_0 n_a c |E_{0a}|^2, \\ \frac{\partial I_a}{\partial z} &= 2\epsilon_0 n_a c \left[E_{0a}^* \frac{\partial E_{0a}}{\partial z} + E_{0a} \frac{\partial E_{0a}^*}{\partial z} \right]. \end{aligned} \quad (47)$$

TABLE I: Band parameter values for Si, masses in free electron mass m_0 , $R_{H,L}^*$ calculated from $(\mu_{H,Ltr}/\epsilon_b^2) \times 13600$ meV, $a_{H,L}^*$ calculated from $(1/\mu_{H,Ltr})\epsilon_b \times 0.0529$ nm, $m_{e,dos}$ calculated from $6^{2/3} (m_{e,tr} m_{e,abs})^{1/3}$.

Parameter	Value	Unit	Reference
$E_g(4.2\text{K})$	1170	meV	[30]
$E_g(300\text{K})$	1124	meV	[30]
$R_H^*(4.2\text{K})$	13.61	meV	
$R_H^*(300\text{K})$	15.65	meV	
$R_L^*(0\text{K})$	8.64	meV	
$R_L^*(300\text{K})$	8.35	meV	
Δ_{LTH}	0.1	meV	[31]
$m_{e,long}(4.2\text{K})$	0.9163	m_0	[32]
$m_{e,long}(300\text{K})$	1.09	m_0	[30]
$m_{e,tr}$	0.1905	m_0	[32]
$m_{e,dos}(4.2\text{K})$	1.04	m_0	
$m_{e,dos}(300\text{K})$	1.12	m_0	
m_{hH}	0.49	m_0	[33]
m_{hL}	0.16	m_0	[33]
$m_{hH}(4.2\text{K})$	0.59	m_0	[30]
$m_{hH}(300\text{K})$	1.15	m_0	[30]
$\mu_{H,long}(4.2\text{K})$	0.319	m_0	
$\mu_{H,long}(300\text{K})$	0.56	m_0	
$\mu_{H,tr}(4.2\text{K})$	0.137	m_0	
$\mu_{H,tr}(300\text{K})$	0.163	m_0	
$\mu_{L,long}(4.2\text{K})$	0.136	m_0	
$\mu_{L,long}(300\text{K})$	0.14	m_0	
$\mu_{L,tr}(4.2\text{K})$	0.087	m_0	
$\mu_{L,tr}(300\text{K})$	0.087	m_0	
$a_H^*(4.2\text{K})$	4.52	nm	
$a_H^*(300\text{K})$	3.86	nm	
$a_L^*(4.2\text{K})$	7.11	nm	
$a_L^*(300\text{K})$	7.235	nm	
$r_{0H}(4.2\text{K})$	0.487	nm	
$r_{0H}(300\text{K})$	0.455	nm	
$r_{0L}(4.2\text{K})$	0.61	nm	
$r_{0L}(300\text{K})$	0.61	nm	
$\epsilon_b(4.2\text{K})$	11.7		
$\epsilon_b(300\text{K})$	11.9		
T_2	0.1	ns	[26]
T_1	8	ns	fitting
$\hbar\omega_{ph}$	40	meV	fitting, [28]

Similar expressions are obtained for I_b , resulting in the following set of coupled equations (45)-(46) we obtain the set of equations

$$\frac{\partial I_a}{\partial z} = -\alpha_2(\omega_a, \omega_a) I_a^2(z) - \alpha_2(\omega_a, \omega_b) I_a(z) I_b(z), \quad (48)$$

$$\frac{\partial I_b}{\partial z} = -\alpha_2(\omega_b, \omega_b) I_b^2(z) - \alpha_2(\omega_b, \omega_a) I_b(z) I_a(z),$$

These equations define the nonlinear absorption coefficients α_2 as

$$\begin{aligned}\alpha_2(\omega_a, \omega_a) &= \frac{\omega_a}{2\epsilon_0 n_a^2 c^2} \chi_{\text{self}}^{(3),I}(\omega_a, \omega_a), \\ \alpha_2(\omega_a, \omega_b) &= \frac{\omega_a}{2\epsilon_0 n_a n_b c^2} \chi_{\text{cross}}^{(3),I}(\omega_a, \omega_b), \\ \alpha_2(\omega_b, \omega_a) &= \frac{\omega_b}{2\epsilon_0 n_a n_b c^2} \chi_{\text{cross}}^{(3),I}(\omega_b, \omega_a), \\ \alpha_2(\omega_b, \omega_b) &= \frac{\omega_b}{2\epsilon_0 n_b^2 c^2} \chi_{\text{self}}^{(3),I}(\omega_b, \omega_b),\end{aligned}\quad (49)$$

where $\chi^{(3),I}$ indicates the imaginary part of $\chi^{(3)}$. The refractive indices $n_a = n(\omega_a)$, $n_b = n(\omega_b)$ are defined by the real parts of the linear susceptibility $\chi^{(1)}$, defined as

$$n_a = \left\{ \left[\epsilon_b \left(1 + \frac{f_1 \Delta_{LT} [\hbar\Omega_{n,em}/E_g - x_a]}{[(\hbar\Omega_{n,em}/E_g) - x_a]^2 + \gamma_2^2} \right) \right] \right\}^{1/2}, \quad (50)$$

with analogous formulas for ω_b and the absorptive term $\hbar\Omega_{n,abs}$. Here, f_1 is the oscillator strength (here for the heavy hole exciton), written as

$$f_{1H} = \frac{\eta_{00H}^3}{[1 + \eta_{00H}(r_{0H}/a_H^*)]^3}, \quad (51)$$

see Eq. (21).

The susceptibilities and, in consequence, the nonlinear absorption coefficients, are composed of 4 components: two corresponding to the contributions of discrete and continuous states, and each of them containing terms related to phonon emission and absorption

$$\alpha_2(\omega_a, \omega_b) = \alpha_{2d}(\omega_a, \omega_b) + \alpha_{2c}(\omega_a, \omega_b), \quad (52)$$

For the discrete states, we only consider the lowest exciton state with $n = 1$, yielding the following form

$$\begin{aligned}\alpha_{2d}(\omega_a, \omega_b) &= -2x_a \gamma_2 \alpha' \left(\frac{T_1}{T_2} \right) \left\{ \frac{\epsilon_b}{n_a n_b} \frac{n_{ph} + 1}{(\hbar\Omega_{1,em}/E_g - x_b)^2 + \gamma_2^2} \right. \\ &\times \frac{\hbar\Omega_{1,em}/E_g}{[(\hbar\Omega_{1,em}/E_g)^2 - x_a^2]^2 + (2\gamma_2 x_a)^2} \\ &+ \frac{\epsilon_b}{n_a n_b} \frac{n_{ph}}{(\hbar\Omega_{1,abs}/E_g - x_a)^2 + \gamma_2^2} \\ &\left. \times \frac{\hbar\Omega_{1,abs}/E_g}{[(\hbar\Omega_{1,abs}/E_g)^2 - x_b^2]^2 + (2\gamma_2 x_b)^2} \right\},\end{aligned}\quad (53)$$

where the constant α' is defined as

$$\begin{aligned}\alpha'(\omega_a, \omega_b) &= 2 \frac{4E_g}{\epsilon_0 \hbar n_a n_b 2c^2 E_g^3} \frac{2M_0^2}{\epsilon_0} [\varphi_{1H}(0)A_1 + \varphi_{1H}(0)B_1] c_{1H}^2 \\ &= 2 \frac{1}{4} \epsilon_0^2 \epsilon_b^2 \pi^2 a_H^{*6} \Delta_{LTH}^2 \times \frac{4}{\pi \epsilon_0 \hbar n_a n_b c^2 E_g^2} \\ &\times [\varphi_{1H}(0)A_1 + \varphi_{1H}(0)B_1] \left(\frac{\eta_H}{a_H^*} \right)^3 \frac{1}{(1 + \eta_H r_{0H}/a_H^*)^2} \\ &= 2 \frac{\pi \epsilon_b^2 \Delta_{LTH}^2 (\eta_H a_H^*)^3 [\varphi_{1H}(0)A_1 + \varphi_{1H}(0)B_1]}{E_g^2 \hbar c^2 n_a n_b (1 + \eta_H r_{0H}/a_H^*)^2}.\end{aligned}$$

The continuum states contribution has the form

$$\alpha_{2c}(\omega_a, \omega_b) = \alpha_{2c,em}(\omega_a, \omega_b) + \alpha_{2c,abs}(\omega_a, \omega_b), \quad (54)$$

where

$$\begin{aligned}\alpha_{2c,em}(\omega_a, \omega_b) &= -\frac{4E_g(n_{ph} + 1)}{\epsilon_0 \hbar n_a n_b c^2} M_0^4 \left(\frac{2\mu_{\parallel H}}{\hbar^2} \right)^2 \frac{1}{4\pi r_0} \frac{T_1}{\hbar} \\ &\times x_a \left(\frac{\sin(\tilde{\kappa}_{a-,em} r_0)}{\tilde{\kappa}_{a-,em} r_0} \right)^2 [\tilde{\kappa}_{b-,em} r_0 + \tilde{\kappa}_{b-,abs} r_0] a_H^{*2} \\ &\times \frac{A_e'' + A_h''}{a_H^{*2}},\end{aligned}\quad (55)$$

$$\begin{aligned}\alpha_{2c,abs}(\omega_a, \omega_b) &= -\frac{4E_g n_{ph}}{\epsilon_0 \hbar n_a n_b c^2} M_0^4 \left(\frac{2\mu_{\parallel H}}{\hbar^2} \right)^2 \frac{1}{4\pi r_0} \frac{T_1}{\hbar} \\ &\times x_a \left(\frac{\sin(\tilde{\kappa}_{a-,abs} r_0)}{\tilde{\kappa}_{a-,abs} r_0} \right)^2 [\tilde{\kappa}_{b-,em} r_0 + \tilde{\kappa}_{b-,abs} r_0] a_H^{*2} \\ &\times \frac{A_e'' + A_h''}{a_H^{*2}}.\end{aligned}\quad (56)$$

The solutions obtained in the two regimes of discrete and continuous states are smoothly connected with the use of hyperbolic tangent function. Using the above formula, we have calculated the 2PA coefficient $\alpha_2(\omega, \omega_b)$ as a function of the energies $\hbar\omega_a + \hbar\omega_b$. The band parameters used in the calculations are listed in Tables I - III.

III. EXPERIMENTAL

We perform optical experiments to determine nonlinear absorption coefficients of silicon to supplement existing data in the literature, spanning a wider range of $x = \frac{\hbar(\omega_a + \omega_b)}{2E_g}$ values. For this purpose, we perform cross correlation experiments, using optical pulses derived from 1-kHz amplified femtosecond laser system (Spitfire Ace, Spectra Physics) system. The laser seeds two optical parametric amplifiers (OPA, TOPAS-Prime,

TABLE II: Anisotropy parameters for Si, excitonic energies calculated from Eq. (19)

Parameter	Value	Unit	$\eta_{00v} = \eta_v$
$\gamma_{aH}(4.2K)$	0.43		1.13
$ E_{1H} (4.2K)$	17.38	meV	
$\gamma_{aH}(300K)$	0.29		1.18
$ E_{1H} (300K)$	21.75	meV	
$\gamma_{aL}(4.2K)$	0.64		1.07
$ E_{1L} (4.2K)$	9.94	meV	
$\gamma_{aL}(300K)$	0.62		1.078
$ E_{1L} (300K)$	9.70	meV	

TABLE III: Thermal electron and hole lengths for Si, and expressions $\varphi_{1H}(0)A_{1H}, B_{1H}$ $\varphi_{2H}(0)A_{2H}, B_{2H}$

Quantity	Value 4.2K	Value 300 K	Reference
λ_{eH}	5.09	0.675	
λ_{hH}	4.70	0.42	
$\varphi_{1H}(0)A_{1H}$	4×1.64	4×0.23	
$\varphi_{1H}(0)B_{1H}$	4×1.57	4×0.155	

Light Conversion), where one OPA is used as a source of near-infrared (NIR) probe radiation between 1150 nm - 1350 nm (1.08 eV - 0.91 eV), producing pulses in the range of 100-150 fs. The signal and idler pulses from the second OPA system are used to generate MIR pump pulses through the process of difference frequency generation (DFG) in the 2480 nm to 4651 nm (0.5 eV - 0.27 eV) range, producing 175-265 fs pulses. The MIR pump is modulated using an optical chopper at a frequency of 500 Hz that is synchronized to the laser output (MC2000B, Thorlabs).

We use a 280 μm thick [100] silicon window (99.999% purity, University Wafer) as the sample target. The MIR and NIR pulses are focused in a non-collinear arrangement on the Si target, using normal incidence for the pump beam and a ~ 20 degree incidence angle for the probe beam. Temporal overlap is controlled through an automated translation stage (GTS150, Newport) in the probe arm, producing a cross-correlation of pump induced probe absorption via NTA. The remaining probe is then attenuated by a 3 OD neutral density filter and detected using a home-built InGaAs photodiode. The modulated change induced by the MIR pump is analyzed by a lock-in amplifier (SR860, Stanford Research Systems). The resulting cross-correlation is then used to extract a nonlinear absorption coefficient α_2 as described by Negres et al. [34]

Figure 1 shows a representative cross correlation and its corresponding fit, and the tabulated data of extracted α_2 values are presented in Table IV. A full description of the data analysis is presented in the Supplemental Materials. Pump-to-probe beam radius ratios were maintained to at least 8:1 as measured by knife edge scan.

TABLE IV: Experimentally obtained values for α_2 in cm/GW

Wavelength (nm)	2480	3295	3755	4220
1150	1.099	0.71	0.823	0.955
1200	0.951	0.638	0.705	0.817
1250	0.846	0.564	0.501	0.481
1350	0.634	0.452	0.385	0.307

The low irradiance of the probe beam in conjunction with the use of a lock-in amplifier ensures that any degenerate two-photon absorption present is excluded from the measured signal. The pump beam is always the longer wavelength beam, minimizing free carrier absorption induced by the probe via three- or four-photon absorption.

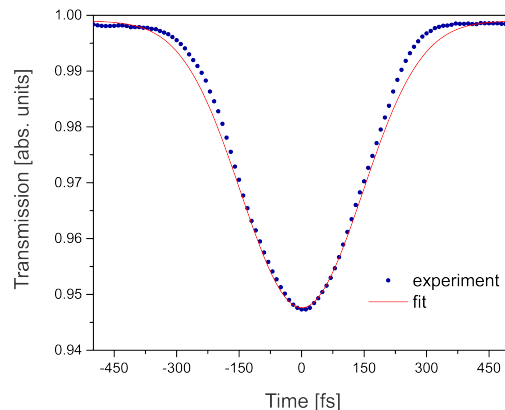


FIG. 1: Exemplary pump probe data and corresponding nonlinear transmittance fit. The photon energies used here are 0.91 eV and 0.376 eV.

IV. RESULTS AND DISCUSSION

The derived form of α_2 that follows from the RDMA approach contains contributions from the two regimes of exciton production, namely the contributions from discrete states and continuum states, see equation (52). Both regimes rely on dipole allowed transitions while considering either the absorption or emission. The discrete regime is visually depicted in Figure 2, which highlights the two-dimensional dispersion of α_2 . The analysis recognizes the presence of a single discrete excitonic state below the band edge, corresponding to the creation of a bound state through absorption of a phonon, $\hbar\Omega_{abs}$, which may provide considerable enhancement to the 2PA process. This is manifested by the presence of resonant denominators for the discrete regime, which can be writ-

ten in simplified form from equation (53) as

$$\alpha_{2d}(\omega_a, \omega_b) \propto \frac{1}{(\hbar\Omega_{abs}/E_g - \hbar\omega_b/E_g)^2 + \gamma_2^2} \times \frac{\hbar\Omega_{em}/E_g}{[(\hbar\Omega_{em}/E_g)^2 - (\hbar\omega_a)^2]^2 + (2\gamma_2\hbar\omega_a)^2} \quad (57)$$

This single state is the only one considered due to the low binding energy of Si, which precludes the formation of bound excitons with higher principal quantum numbers. When $\hbar\omega_b/\hbar\omega_a$ is detuned away from degeneracy, we observe an increase of α_2 that is as much as $5\times$ the equivalent degenerate response, amplifying the process as it becomes doubly resonant with the lowest discrete state and the edge of the continuum at room temperature. This behavior is evident in the corners of Figure 2. While smaller in magnitude, the $\hbar\Omega_{abs}$ state provides additional enhancement when at least one incident photon approaches this energy. An alternate resonance condition exists when both photons are resonant with the discrete exciton level at approximately 95% of the band gap. This is a singly resonant process where the intermediate state is the lowest excitonic state, providing some enhancement to the two-photon process.

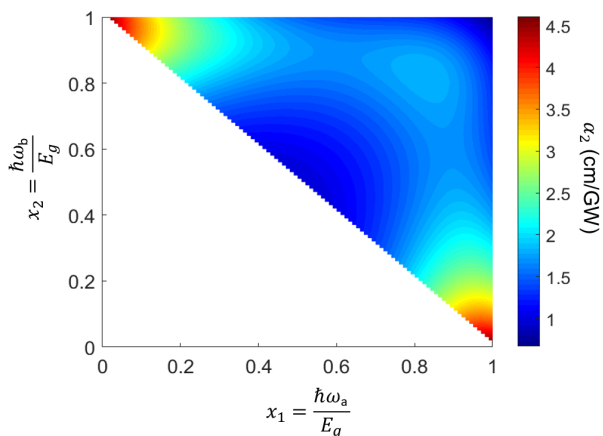


FIG. 2: Scaling behavior of the two photon absorption coefficient α_2 as a function of normalized photon energy while both photons are below the gap.

If the the energy of the incident photons exceeds the bandgap energy, then the two-photon absorption process proceeds entirely via continuum states. This can be accessed by either phonon absorption or emission, and the nonlinear absorption coefficient has the form as in equation (54). Beyond the band edge, the continuum causes α_{2c} to further increase up to the point where the energy of at least one of the photons has enough energy to reach the direct gap of silicon at $E_g = 3.43$ eV. This increase is due to the oscillatory behavior of the linear coherent amplitude of the exciton density $Y^{(1)}$, which contributes to the induced polarization of the medium in order for two-photon absorption to occur.

To validate the performance of the model, we first apply it to explain an experimental data set of the degenerate two-photon (DTA) cross section obtained from an open aperture Z-scan reported in Ref [35]. As can be seen in Figure 3(a), α_2 for the DTA process reveals a resonance-like behavior as a function of photon energy. A previous analysis using a model for direct transitions, corrected for the center of mass energy when phonon scattering is involved [36], reproduced the general dependence of α_2 on the photon energy, but it failed to predict the observed resonance structure. The RDMA approach (indicated by the solid line in Figure 3), on the other hand, predicts a resonant behavior when the individual photon energy approaches the energy of the discrete exciton state, resulting in a satisfactory description of the data. When the photon energy exceeds the band gap, the role of the bound exciton states decreases and instead the response is largely dictated by continuum states, which results in a slight decrease of α_2 . Note that only the dephasing times in the RDMA analysis are fitting parameters, while all other parameters are obtained from the tabulated values shown Tables I-III.

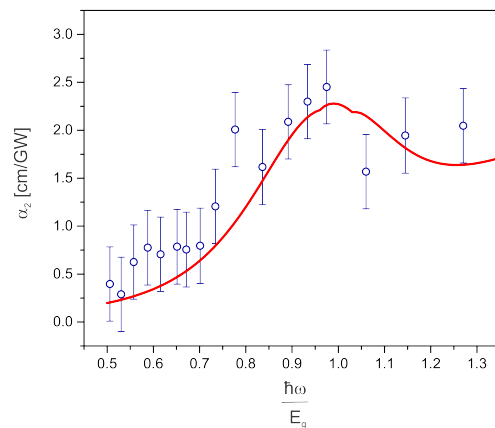


FIG. 3: Scaling of the degenerate two-photon absorption coefficient α_2 as a function of $x = \hbar\omega/E_g$. Squares are obtained from Ref [35] and thick solid line results from the RDMA analysis of two-photon absorption.

We next use the model to describe the energy scaling of the NTA coefficient as measured in Ref [23], which encompasses a normalized photon energy range of $x = \hbar(\omega_a + \omega_b)/2E_g = 1.1 - 2$. In addition, we apply the model to fit a new data set that we have collected for a non-degenerate energy ratio in the $\hbar\omega_a/\hbar\omega_b = 2-4$ range, corresponding to pump photon energies of 0.294 eV–0.5 eV and probe energies of 0.91 eV–1.08 eV. Both data sets, shown in Figures 4 and 5, correspond to a normalized equivalent energy range of $x = 0.55 - 0.8$, but have different levels of non-degeneracy, thus complementing each other. The theoretical predictions for α_2 are in good agreement with both experimental data sets. The most

notable feature in the normalized photon energy curve is the appearance of a peak, which the model attributes to the presence of the bound exciton resonance. The position of this peak shifts in accordance with the energy tuning of the lower energy pump photon, and its magnitude is largely dictated by the damping terms in the resonant denominators of α_{2d} . However, this resonant behavior is significantly different from what is reported in [23], where the theoretical predictions made anticipate a quasi-linear scaling of α_2 as a function of the normalized photon energy. Future work may include performing NTA experiments to verify the behavior of α_2 and the influence of continuum states above the band edge, such as can be obtained with a two-color Z-scan.

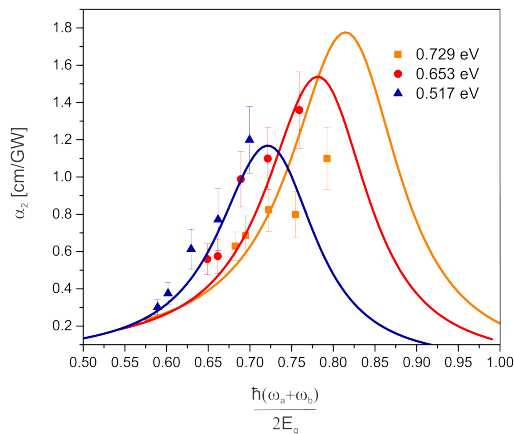


FIG. 4: Scaling of the non-degenerate two-photon absorption coefficient α_2 as a function of the normalized equivalent energy. Experimental data points are obtained from Ref [23] and thick solid lines represent the results from the RDMA analysis. Different colors correspond to different non-degeneracy energy ratios $\hbar\omega_a/\hbar\omega_b$.

This work is a significant departure from the conventional understanding of the two-photon absorption process in semiconductors. Previous methods have described the 2PA absorption process in terms of transition rate matrix elements based on electron band states, where significantly nondegenerate photons become resonant with the interband transition and an intraband transition simultaneously. Within the framework of the RDMA, the defining feature of the absorption process is the ability to produce either bound or free excitons within the material. Tracking the formation of excitons allows the RDMA to yield general expressions for semiconducting materials with low binding energies, i.e. only the lowest discrete state needs to be considered. These results are analytical in that there is no parametrization done to provide free variables for fitting. The only variability results from loosely determined material parameters, namely the relaxation times T_1 and T_2 .

It is possible to apply this analysis to direct gap two-

photon transitions as well, which omits the involvement of phonon absorption or emission processes in the final equations. The RDMA also accounts for the physical realities of material anisotropy and relaxation mechanisms that are often added phenomenologically elsewhere. Bolstered by the excellent agreement between theory and experiment over a wide range of photon energies and non-degeneracy ratios, we believe that the current description provides a deeper insight into two-photon absorption process in semiconducting materials.

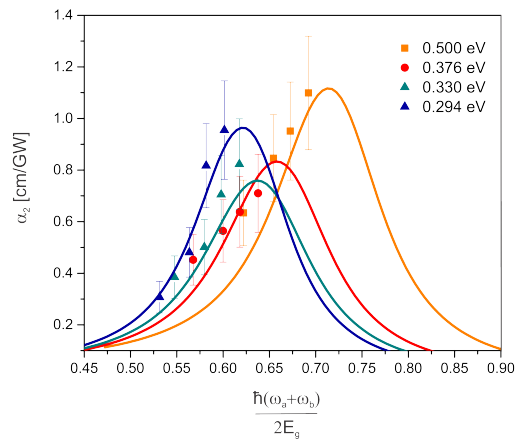


FIG. 5: Scaling of the non-degenerate two-photon absorption coefficient α_2 as a function of the normalized equivalent energy. Data points indicate experimental results and thick solid lines represent the results from the RDMA analysis. Different colors correspond to different non-degeneracy energy ratios $\hbar\omega_a/\hbar\omega_b$.

V. CONCLUSION

We employed the RDMA approach to elucidate two-photon absorption (2PA) in indirect gap semiconductors, employing silicon as the representative material. Our methodology, in contrast to existing models for 2PA in semiconductors, uniquely incorporates a detailed description of DTA (direct two-photon absorption) and NTA (non-direct two-photon absorption) through the production of excitons, a physical insight often overlooked in prior analyses. The approach allows the computation of the non-degenerate two-photon absorption coefficient, capturing the influence of both bound and free excitonic states within the material. In addition, the RDMA enables the inclusion of the effects of phonon-assisted transitions and material anisotropy. According to our model, the two-photon absorption process in silicon intensifies as the energy of individual incident photons, while below the gap, approaches the single bound excitonic state. This prediction aligns with recently obtained experimental NTA absorption data, casting new light on the interpretation of published DTA data in bulk silicon. Above

the gap, the 2PA process primarily occurs through the continuum of free states, providing a satisfactory description of the DTA data across a wide photon energy range ($\hbar\omega/E_g = 0.5 - 1.3$). Last, but not least, the analysis outlined using the RDMA can be generalized and readily applied to other indirect gap materials by adjusting the necessary material values. Furthermore, the model can be adapted to describe direct transitions by excluding the involvement of phonon modes to complete the transition.

ACKNOWLEDGMENTS

DAF and EOP acknowledge support of the Chan-Zuckerberg Initiative and the National Health Institute, grant R21-GM141774. AS acknowledges the support of the Air Force Office of Scientific Research (AFOSR) through the grant FA9550-23-1-0267.

-
- [1] W. Denk, J. H. Strickler, and W. W. Webb, Two-photon laser scanning fluorescence microscopy, *Science* **248**, 73 (1990).
- [2] S. Maruo, O. Nakamura, and S. Kawata, Three-dimensional microfabrication with two-photon-absorbed photopolymerization, *Opt. Lett.* **22**, 132 (1997).
- [3] S. Kawata, H. Sun, T. Tanaka, and K. Takada, Micromachines can be created with higher resolution using two-photon absorption, *Nature* **412**, 697 (2001).
- [4] D. A. Parthenopoulos and P. M. Rentzepis, Three-dimensional optical storage memory, *Science* **245**, 843 (1989).
- [5] W. Rudolph, M. Sheik-Bahae, A. Bernstein, and L. F. Lester, Femtosecond autocorrelation measurements based on two-photon photoconductivity in ZnSe, *Opt. Lett.* **22**, 313 (1997).
- [6] S. Lochbrunner, P. Huppmann, and E. Riedle, Crosscorrelation measurements of ultrashort visible pulses: comparison between nonlinear crystals and SiC photodiodes, *Optics Commun.* **184**, 321 (2000).
- [7] D. A. Fishman, C. M. Cirloganu, S. Webster, L. A. Padilha, M. Monroe, D. J. Hagan, and E. W. Van Stryland, Sensitive mid-infrared detection in wide-bandgap semiconductors using extreme non-degenerate two-photon absorption, *Nat. Phot.* **5**, 561 (2011).
- [8] J. Fang, Y. Wang, M. Yan, E. Wu, K. Huang, and H. Zeng, Highly Sensitive Detection of Infrared Photons by Nondegenerate Two-Photon Absorption Under Mid-infrared Pumping, *Phys. Rev. Appl.* **14**, 064035 (2020).
- [9] D. Knez, A. M. Hanninen, R. C. Prince, E. O. Potma, and D. A. Fishman, Infrared chemical imaging through non-degenerate two-photon absorption in silicon-based cameras, *Light: Science & Applications* **9**, 125 (2020).
- [10] E. O. Potma, D. Knez, M. Ettenberg, M. Wizeman, H. Nguyen, T. Sudol, and D. A. Fishman, High-speed 2D and 3D mid-IR imaging with an InGaAs camera, *APL Photonics* **6**, 096108 (2021).
- [11] W. Liu, D. Shen, G. Zhao, H. Yan, Z. Zhou, and W. Wan, Spatial narrowing of two-photon imaging in a silicon CCD camera, *IEEE Phot. Technol. Lett.* **34**, 459 (2022).
- [12] B. S. Wherrett, Scaling rules for multiphoton interband absorption in semiconductors, *J. Opt. Soc. Am. B* **1**, 67 (1984).
- [13] M. Sheik-Bahae, D. Hutchings, D. Hagan, and E. Van Stryland, Dispersion of bound electron nonlinear refraction in solids, *IEEE J. of Quantum Electronics* **27**, 1296 (1991).
- [14] D. C. Hutchings and E. W. Van Stryland, Nondegenerate two-photon absorption in zinc blende semiconductors, *J. Opt. Soc. Am. B* **9**, 2065 (1992).
- [15] G. Jalbert, B. Koiller, H. S. Brandi, and N. Zagury, Dressed bands approach for multi-photon transitions in solids, *J. Phys. C: Solid State Physics* **19**, 5745 (1986).
- [16] D. C. Hutchings and B. S. Wherrett, Theory of anisotropy of two-photon absorption in zinc-blende semiconductors, *Phys. Rev. B* **49**, 2418 (1994).
- [17] C. Aversa, J. E. Sipe, M. Sheik-Bahae, and E. W. Van Stryland, Third-order optical nonlinearities in semiconductors: The two-band model, *Phys. Rev. B* **50**, 18073 (1994).
- [18] C. Aversa and J. E. Sipe, Nonlinear optical susceptibilities of semiconductors: Results with a length-gauge analysis, *Phys. Rev. B* **52**, 14636 (1995).
- [19] W.-R. Hannes and T. Meier, Higher-order contributions and nonperturbative effects in the nondegenerate nonlinear optical absorption of semiconductors using a two-band model, *Phys. Rev. B* **99**, 125301 (2019).
- [20] M. Dinu, Dispersion of phonon-assisted nonresonant third-order nonlinearities, *IEEE J. of Quantum Electronics* **39**, 1498 (2003).
- [21] M. Dinu, F. Quochi, and H. Garcia, Third-order nonlinearities in silicon at telecom wavelengths, *Appl. Phys. Lett.* **82**, 2954 (2003).
- [22] A. Hayat, P. Ginzburg, and M. Orenstein, Infrared single-photon detection by two-photon absorption in silicon, *Phys. Rev. B* **77**, 125219 (2008).
- [23] S. Faryadras, N. Cox, D. J. Hagan, and E. W. Van Stryland, Non-degenerate two-photon absorption spectroscopy of bulk silicon, in *2021 IEEE Research and Applications of Photonics in Defense Conference (RAPID)* (2021) pp. 1-2.
- [24] S. Zielińska-Raczyńska, G. Czajkowski, K. Karpiński, and D. Ziemkiewicz, Nonlinear optical properties and self-kerr effect of rydberg excitons, *Phys. Rev. B* **99**, 245206 (2019).
- [25] C. Morin, J. Tignon, J. Mangeney, S. Dhillon, G. Czajkowski, K. Karpiński, S. Zielińska-Raczyńska, D. Ziemkiewicz, and T. Boulier, Self-Kerr effect across the yellow Rydberg series of excitons in Cu₂O, *Phys. Rev. Lett.* **129**, 137401 (2022).
- [26] M. A. Green, Improved value for the silicon free exciton binding energy, *AIP Advances* **3**, 112104 (2013).
- [27] A. Valentin, J. Sée, S. Galdin-Retailleau, and P. Dollfus, Study of phonon modes in silicon nanocrystals using the adiabatic bond charge model, *Journal of Physics: Condensed Matter* **20**, 145213 (2008).
- [28] D. S. Kim, H. L. Smith, J. L. Niedziela, C. W. Li, D. L. Abernathy, and B. Fultz, Phonon anharmonicity in silicon from 100 to 1500 K, *Phys. Rev. B* **91**, 014307 (2015).

- [29] F. Bassani and G. P. Parravicini, *Electronic States and Optical Transitions in Solids* (Pergamon Press, Oxford, 1975).
- [30] W. H. Strehlow and E. L. Cook, Compilation of Energy Band Gaps in Elemental and Binary Compound Semiconductors and Insulators, *Journal of Physical and Chemical Reference Data* **2**, 163 (2009).
- [31] G. Czajkowski, F. Bassani, and A. Tredicucci, Polaritonic effects in superlattices, *Phys. Rev. B* **54**, 2035 (1996).
- [32] D. Palmer, www.semiconductors.co.uk.
- [33] J. Singh, *Physics of semiconductors and their heterostructures*, McGraw-Hill series in electrical and computer engineering (McGraw-Hill, New York, 1993).
- [34] R. Negres, J. Hales, A. Kobaykov, D. Hagan, and E. Van Stryland, Experiment and analysis of two-photon absorption spectroscopy using a white-light continuum probe, *IEEE Journal of Quantum Electronics* **38**, 1205 (2002).
- [35] A. D. Bristow, N. Rotenberg, and H. M. van Driel, Two-photon absorption and Kerr coefficients of silicon for 850–2200 nm, *Appl. Phys. Lett.* **90**, 191104 (2007).
- [36] H. Garcia and R. Kalyanaraman, Phonon-assisted two-photon absorption in the presence of a dc-field: the nonlinear Franz–Keldysh effect in indirect gap semiconductors, *Journ. of Phys. B: Atomic, Molecular and Optical Physics* **39**, 2737 (2006).